not all the possible ones: in fact, the fade durations for which the attenuation does not reach $S + dS$ dB are excluded.

The loss of memory is also observable in the scattergram $|R|$ against D shown in Fig. 3, for $S = 2$ dB. This behaviour is

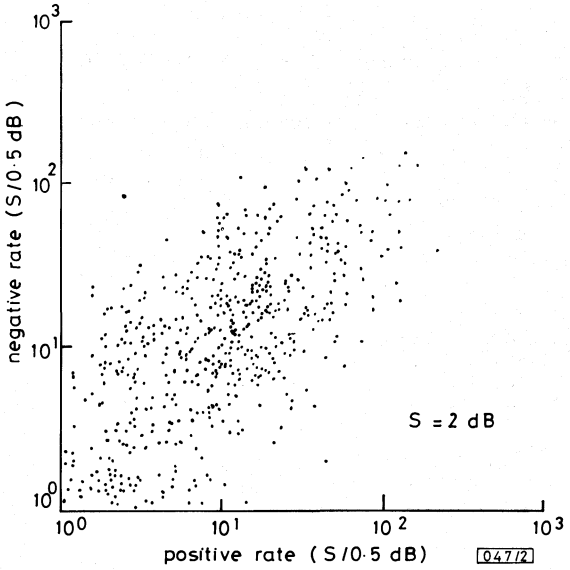

Fig. 2

Table 2 VALUES OF PARAMETERS OF REGRESSION $R^- = a(R^+)^b$ FOR DIFFERENT THRESHOLDS

S	$a = \exp(m)$	b	Correlation coefficient
dB			
2	1·898	0·9354	0·6451
3	1·648	1·0476	0·4965
5	1·501	0·9955	0·4029
7	1·526	0·9418	0·4269

Table 3 VALUES OF PARAMETERS OF REGRESSION $|R| = aD^b$ FOR DIFFERENT THRESHOLDS

S	a	b	Correlation coefficient
dB			
2	1·495	0·4293	0·576
3	1·317	0·7621	0·455
5	1·237	0·8226	0·385
7	1·195	0·7871	0·350

also confirmed by the joint analysis of successive durations and intrafades on the same database, discussed in Reference 4.

Note that, in any case, rates are not independent of the fade duration as, obviously, each rate and their sum cannot exceed the corresponding fade duration.

Similar behaviour is also found for higher thresholds.

Table 3 gives the parameters of logarithmic regression lines between $|R|$ and D for the four thresholds.

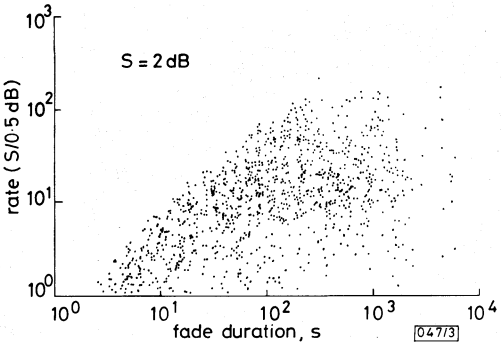

Fig. 3

Conclusions: The joint analysis of positive and negative rates of change and the in-between duration of fade shows that medium-to-low correlation exists between any two variables.

Positive and negative rates of change, conditioned to the threshold, are statistically alike and are well described by log-normal distributions.

E. MATRICCIANI
M. MAURI
A. PARABONI

Dipartimento di Elettronica
Politecnico di Milano
Piazza Leonardo Da Vinci 32
20133 Milano, Italy

10th July 1986

References

1 MATRICCIANI, E.: 'Rate of change of signal attenuation from Sirio at 11·6 GHz', *Electron. Lett.*, 1981, **17**, pp. 139–141
2 MATRICCIANI, E.: 'Effects of filtering on rate of change of rain-induced attenuation', *ibid.*, 1982, **18**, pp. 477–478
3 CARASSA, F., MAURI, M., and PARABONI, A.: 'Attenuation statistics in Italy as measured by the Sirio satellite during its five year lifetime', *IEEE Trans.*, 1984, **AP-32**, pp. 1251–1255
4 MATRICCIANI, E., and MAURI, M.: 'Rain attenuation successive fade durations and time intervals between fades in a satellite-earth link', *Electron. Lett.*, 1986, **22**, pp. 656–658

PERFORMANCE BOUNDS OF RATE-½ CONVOLUTIONAL CODES WITH QPSK ON RAYLEIGH FADING CHANNEL

Indexing terms: Codes, Telecommunications, Convolution

An analytic expression for the bit error probability upper bounds of rate-½ convolutional codes in conjunction with QPSK modulation and maximum-likelihood Viterbi decoding on the fully interleaved Rayleigh fading channel is presented. The given expression is evaluated numerically for selected rate-½ optimum convolutional codes together with QPSK.

Introduction: The performance of rate-½ short-constraint-length convolutional codes in conjunction with BPSK modulation and various kinds of maximum-likelihood (ML) Viterbi decoding on Rician-Rayleigh fading channels has been discussed in detail.[1–3] It has been found that the ML Viterbi decoder which makes perfect channel measurements, channel amplitude and phase gives the best performance. However, with BPSK modulation the code redundancy introduced by convolutional coding represents a bandwidth sacrifice in that the ratio of required bandwidth to information rate is increased. To avoid this sacrifice in bandwidth efficiency and also provide effective error protection, QPSK modulation could be used instead. This letter is concered with the bit error probability performance of rate-½ convolutional codes in conjunction with QPSK modulation and ML Viterbi decoding which makes perfect channel measurements on the fully interleaved Rayleigh fading channel. An analytical expression for the bit error probability upper bounds for rate-½ optimum convolutional codes with constraint lengths $k = 3$ to 7 together with QPSK are evaluated.

System model: The system under consideration is shown in Fig. 1. To compute the error probability the channel is represented by a discrete-time model where the ith input is given by

$$x_i = \exp(j\theta_i) \Big|_{\theta_i} \in \{0, \pi/2, \pi, 3\pi/2\} \quad (1)$$

and the corresponding normalised matched filter output after deinterleaving is

$$y_i = \sqrt{(E_s/N_0)}a_i x_i + N_i \tag{2}$$

where $\{N_i\}$ is an independent identically distributed (IID) noise sequence of complex Gaussian variates with zero mean

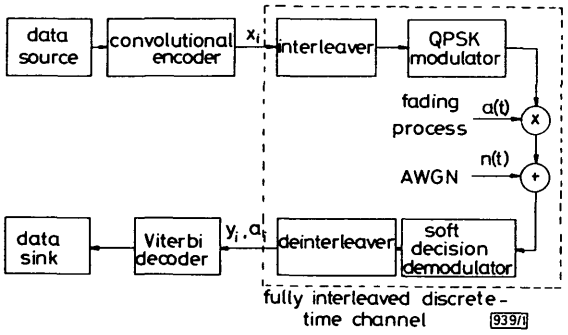

Fig. 1 *Block diagram of system under consideration*

and unit variance. $\{a_i\}$, with a_i representing the value of the amplitude fading process $a(t)$ throughout the ith signalling interval, is an IID sequence of random variates with distribution

$$f(a_i) = 2a_i e^{-a_i^2} \tag{3}$$

and E_s/N_0 is the received signal/noise ratio (SNR) per received symbol, which equals the received SNR per bit, E_b/N_0, in this case, where E_b is the energy per input bit. In addition to y_i, the Viterbi decoder is also supplied with the channel amplitude a_i from a channel estimator.

Pairwise error probability: The pairwise error probability between the transmitted sequence $\boldsymbol{x} = \{x_i\}$ and the estimated sequence $\boldsymbol{x} = \{\hat{x}_i\}$ is now developed. Given the received sequences $\boldsymbol{y} = \{y_i\}$ and $\boldsymbol{a} = \{a_i\}$, the ML decision rule for the Viterbi decoder which makes perfect amplitude measurement implies that

$$P_r(\boldsymbol{y} \mid \boldsymbol{x}, \boldsymbol{a}) < P_r(\boldsymbol{y} \mid \hat{\boldsymbol{x}}, \boldsymbol{a}) \quad \text{when} \quad \hat{\boldsymbol{x}} \neq \boldsymbol{x} \tag{4}$$

Since $\{x_i\}$, $\{\hat{x}_i\}$ and $\{a_i\}$ are IID sequences, eqn. 4 can be manipulated to give

$$\sum_i a_i y_i (x_i - \hat{x}_i)^* + a_i y_i^* (x_i - \hat{x}_i) < 0 \tag{5}$$

where * denotes the complex conjugate. Without loss of generality we may assume that, in the transmitted sequence $\boldsymbol{x}$, $x_i = +1$ for all i (corresponding to the all-zero message). If $\hat{\boldsymbol{x}}$ differs from $\boldsymbol{x}$ in exactly k symbols, and there are k_1 symbols

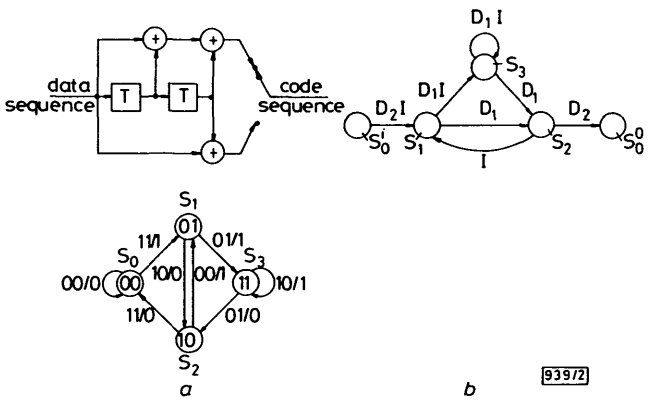

Fig. 2

a Rate-$\frac{1}{2}$, $k = 3$ code and its state diagram
b Modified state diagram code in (*a*) with Gray mapping into QPSK; augmented generating function:

$$T(D_1, D_2, I) \equiv S_0^o/S_0^i = \frac{D_1 D_2^2 I}{1 - 2D_1 I}$$

with value $\pm j$ and k_2 symbols with value -1, then eqn. 5 is equivalent to

$$U = \sum_{l=1}^{k_1} a_l[\sqrt{(E_b/N_0)}a_l + \text{Re}\,(N_l) \mp \text{Im}\,(N_l)] + 2\sum_{m=1}^{k_2} a_m[\sqrt{(E_b/N_0)}a_m + \text{Re}\,(N_m)] < 0 \tag{6}$$

where Re (N_i) and Im (N_i) are the quadrature components of complex noise N_i described in eqn. 2. Making use of the inequality $Q(x) \leq \frac{1}{2}\exp(-x^2/2)$, we have the conditional pairwise error probability

$$\begin{aligned} P_{k_1 k_2}(E \mid \boldsymbol{a}) &= P_r(U < 0) \\ &= Q\left\{\sqrt{\left[\frac{E_b}{N_0}\left(\sum_{l=1}^{k_1} a_l^2\right) + 2\sum_{m=1}^{k_2} a_m^2\right]}\right\} \\ &\leq \frac{1}{2}\exp\left(-\frac{E_b}{2N_0}\sum_{l=1}^{k_1} a_l^2\right)\exp\left(-\frac{E_b}{N_0}\sum_{m=1}^{k_2} a_m^2\right) \end{aligned} \tag{7}$$

where

$$Q(x) = \int_x^\infty \frac{1}{\sqrt{(2\pi)}} e^{-w^2/2}\, dw$$

Since a_i is Rayleigh-distributed, $q_n \equiv \sum_{i=1}^{k_n} a_i^2$ is a χ^2-distributed random variable. Thus

$$E[\exp(wq_n)] = \frac{1}{(1-w)^{k_n}} \tag{8}$$

The unconditional pairwise error probability hence becomes

$$\begin{aligned} P_{k_1 k_2} &= E_A[P_{k_1 k_2}(E \mid \boldsymbol{a})] \\ &\leq \frac{1}{2}\left(\frac{1}{1 + E_b/2N_0}\right)^{k_1}\left(\frac{1}{1 + E_b/N_0}\right)^{k_2} \end{aligned} \tag{9}$$

Performance upper bound: At this point the generating function union bounding approach initiated by Viterbi[4] is applied to derive the bit error probability upper bound. For a convolutional code with QPSK the augmented generating function denoted by $P(D_1, D_2, I)$ can be obtained in the conventional manner, except that the weight label of the branches on the state diagram should be properly modified. For illustrative purposes, an example is given in Fig. 2. In terms of $T(D_1,$

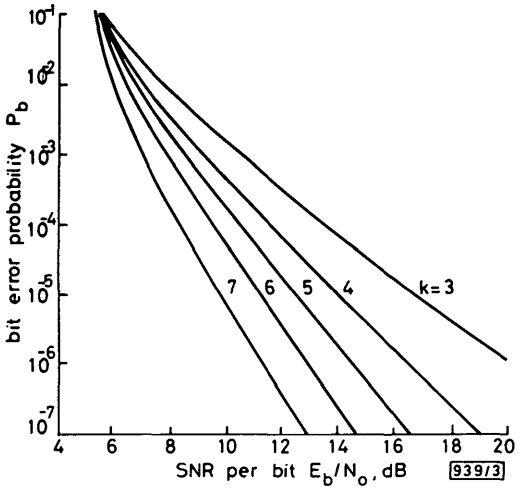

Fig. 3 *Computed upper bounds for selected rate-$\frac{1}{2}$ codes with QPSK on fully interleaved Rayleigh fading channel*

k is the constraint length

D_2, I) the bit error probability P_b for rate-$\frac{1}{2}$ convolutional codes with QPSK modulation is upper-bounded by

$$P_b \leq \frac{1}{2} \left. \frac{\partial T(D_2, D_1, I)}{\partial I} \right|_{I=1} \qquad (10)$$

$$D_1 = \frac{1}{1 + E_b/2N_0} \qquad D_2 = \frac{1}{1 + E_b/N_0}$$

This expression for P_b is numerically evaluated and is plotted in Fig. 3 for the selected rate-$\frac{1}{2}$ optimum convolutional codes with constraint lengths $k = 3$ to 7 and with Gray mapping into QPSK.

Conclusion: For rate-$\frac{1}{2}$ convolutional codes with QPSK on a Rayleigh fading channel, the derived analytic expression is a weak upper bound on the bit error probability. However, the approach utilised here can be extended to convolutional codes with M-ary PSK modulation on Rician fading channels. A generalised expression for the tight bit error probability upper bounds is under investigation.

YUH-LONG CHEN
CHE-HO WEI

Institute of Electronics
National Chiao Tung University
Hsin-Chu, Taiwan, Republic of China

16th June 1986

References

1 MODESTINO, J. W., and MUI, S. Y.: 'Convolutional code performance in the Rician fading channel', *IEEE Trans.*, 1976, **COM-24**, pp. 592–606
2 HAGENAUER, J.: 'Viterbi decoding of convolutional codes for fading- and burst-channel'. Proceedings of international Zurich seminar on digital communications, Zurich, 1980, pp. G2.1-7
3 DUNHAM, J. G., and TZOU, K.-H.: 'Performance bounds for convolutional codes on Rician fading channels'. Proceedings of international conference on communications, Denver, 1981, pp. 12.4.1-5
4 VITERBI, A. J.: 'Convolutional codes and their performance in communications', *IEEE Trans.*, 1971, **COM-19**, pp. 751–771

COAXIALLY MOUNTED 67 GHz BANDWIDTH InGaAs PIN PHOTODIODE

Indexing terms: Photoelectric devices, Photodiodes

We report high-speed measurements of an InGaAs PIN photodiode in a millimetre-wave coaxial mount. The photodiode has an impulse response (including diode, parasitics and connector) of 9 ps FWHM and a 3 dB bandwidth of 67 GHz. This is the largest bandwidth reported to date for a photodiode in a coaxial mount with a connector.

Wideband photodiodes are important components for multigigabit/second optical systems operating in the 0·8 μm and 1·3 μm to 1·55 μm wavelength ranges. To attain high-speed performance, it is necessary that the active region of the photodiode have a small area (to minimise capacitance) and be thin (to minimise carrier transit times).[1–4] In addition, it is necessary that electrical parasitics associated with the device package be kept small. To this end, the chip is usually mounted in a microstrip,[1,2] coaxial[3,4] or waveguide[5] fixture, preferably with some form of connector for convenient connection to test instrumentation. The highest bandwidth reported to date for an InGaAs PIN detector, with a 50 Ω coaxial connector and an internal biasing circuit, is 36 GHz.[4] A similar device, in a 25 Ω hybrid circuit, has shown an impulse response of 10 ps FWHM.[6] Responses at frequencies to 60 GHz have been achieved using waveguide test fixtures,[5] but separate photodiodes and waveguides are required to cover the full 26·5 GHz to 60 GHz measurement range.[5] This letter reports bandwidth measurements of a PIN photodiode in a coaxial mount. The photodiode shows a response extending from DC to millimetre-wave frequencies, with a 3 dB bandwidth of 67 GHz and an impulse response of 9 ps FWHM. This is the fastest response reported to date for a photodiode in a coaxial mount with a connector.

The PIN photodiode used here is a back-illuminated mesa structure with an active area of approximately 150 μm^2 and an intrinsic layer thickness of approximately 0·5 μm. Further details of the photodiode structure are given in Reference 3. The chip was mounted on a small, low-inductance L-shaped bracket provided with a hole to allow back-illumination of the intrinsic region. The mesa contact on the chip was connected directly via a short (250 μm) length of low-inductance gold mesh to the centre pin of a commercial coaxial-to-microstrip transition (Wiltron K-connector). The chip was from the same wafer as those of References 4–6, and the mounting was nominally identical to that of Reference 4.

The electrical parasitics of the photodiode were determined from a series of network analyser reflection coefficient measurements at frequencies up to 10 GHz. These measurements were carried out using (i) a bare K-connector and (ii) a K-connector with the photodiode mounted. From these measurements, the parasitic capacitance shunting the depletion region was determined to be 0·05 pF at 5 V reverse bias, in agreement with previous estimates for a similar device.[4] The series inductance of the gold mesh is approximately 0·2 nH.

The response of the photodiode was measured at a wavelength of 1·3 μm by electro-optic sampling in GaAs.[7] The sampler comprised a 50 Ω microstrip line deposited on a semi-insulating GaAs substrate and mounted in a package which was equipped with K-connectors of opposite sex to the photodiode package. The photodiode was connected directly to one end of the sampler, while the other end of the sampler was terminated with a bias tee and a 50 Ω load. Note that this experimental arrangement gives the response of the diode, parasitics and coaxial connector, but enables the response of the bias network to be excluded. We believe that this is a major factor responsible for the improvement in our measured bandwidth over that reported in Reference 4.

A mode-locked 1·3 μm InGaAsP injection laser operating at a repetition rate of 3·7 GHz was used both to pump the photodiode and to probe the electro-optic sampler. An important feature of the measurement system is that the effect of the nonzero pulsewidth of the mode-locked laser can be deconvolved from the measured data if the intensity autocorrelation function of the laser is known.[8] In the present work, the autocorrelation was measured by conventional second-harmonic generation techniques, using a nonlinear $LiIO_3$ crystal. The measured autocorrelation width was 17 ps FWHM. The uncertainty in the deconvolved photodiode response was approximately ±2 ps, due to the finite signal/noise ratio of the measurement. Further details of the measurement technique are presented in Reference 7.

Fig. 1 shows the measured impulse response of the photodiode when biased at 5 V. The broken curve is the response as obtained directly from electro-optic sampling, while the solid curve is the photodiode response after deconvolving the auto-

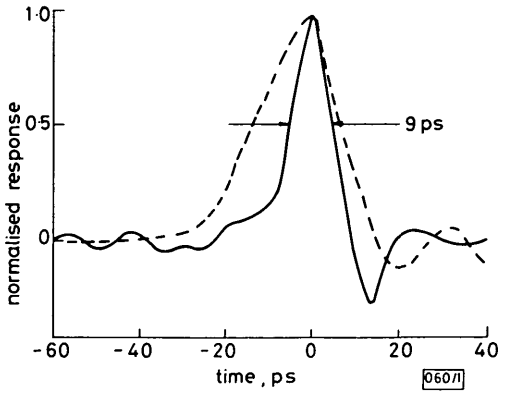

Fig. 1 *Measured impulse response of photodiode*
Broken curve: sampled signal
Solid curve: deconvolved response